Probes of Hydrogen Tunneling with Horse Liver Alcohol Dehydrogenase at Subzero Temperatures†

Shiou-chuan Tsai‡ and Judith P. Klinman*

Department of Chemistry, University of California at Berkeley, Berkeley, California 94720

Received September 1, 2000; Revised Manuscript Received November 22, 2000

ABSTRACT: The temperature dependence of steady-state kinetics has been studied with horse liver alcohol dehydrogenase (HLADH) using protonated and deuterated benzyl alcohol as substrates in methanol/water mixtures between +3 and −50 °C. Additionally, the competitive isotope effects, k_H/k_T and k_D/k_T, were measured. The studies indicate increasing kinetic complexity for wild-type HLADH at subzero temperatures. Consistent with earlier findings at 25 °C [Bahnson et al. (1993) *Biochemistry 31*, 5503], the F93W mutant shows much less kinetic complexity than the wild-type enzyme between 3 and −35 °C. An analysis of noncompetitive deuterium isotope effects and competitive tritium isotope effects leads to the conclusion that the reaction of F93W involves substantial hydrogen tunneling down to −35 °C. The effect of methanol on kinetic properties for the F93W mutant was analyzed, showing a dependence of competitive KIEs on the NAD^+ concentration. This indicates a more random bi−bi kinetic mechanism, in comparison to an ordered bi−bi kinetic mechanism in water. Although MeOH also affects the magnitude of the reaction rates and, to some extent, the observed KIEs, the ratio of ln k_H/k_T to ln k_D/k_T for primary isotope effects has not changed in methanol, and we conclude little or no change in kinetic complexity. Importantly, the degree of tunneling, as shown from the relationship between the secondary k_H/k_T and k_D/k_T values, is the same in water and MeOH/water mixtures, implicating similar trajectories for H transfer in both solvents. In a recent study of a thermophilic alcohol dehydrogenase [Kohen et al. (1999) *Nature 399*, 496], it was shown that decreases in temperatures below a transition temperature lead to decreased tunneling. This arises because of a change in protein dynamics below a break point in enzyme activity [Kohen et al. (2000) *J. Am. Chem. Soc. 122*, 10738−10739]. For the mesophilic HLADH described herein, an opposite trend is observed in which tunneling increases at subzero temperatures. These differences are attributed to inherent differences in tunneling probabilities between 0 and 100 °C vs subzero temperatures, as opposed to fundamental differences in protein structure for enzymes from mesophilic vs thermophilic sources. We propose that future investigations of the relationship between protein flexibility and hydrogen tunneling are best approached using enzymes from thermophilic sources.

The traditional analyses of enzymes and their complexes with either substrates or substrate analogues provide a static framework for the understanding of catalysis. Whereas protein conformational changes play a role in many enzyme reactions, it has been commonly assumed that dynamical motions within the protein backbone do not actively participate in the bond making/breaking processes. In recent years, it has been increasingly recognized that enzyme-catalyzed hydrogen-transfer processes are accompanied by varying degrees of tunneling under the physiological conditions of the catalyst (*1*). Importantly, hydrogen tunneling is highly distance-dependent, such that modest changes in protein structure may be expected to affect the tunneling behavior very significantly (*2*−*6*). During the last year, several studies have been completed in which the observed properties of tunneling as a function of temperature point toward an essential dynamic component in efficient H tunneling for an alcohol dehydrogenase from a thermophilic source (*7*, *8*).

In this paper, we turn to the use of cryoenzymology, in an effort to examine the effect of subzero temperatures on the hydrogen-transfer properties of the mesophilic horse liver alcohol dehydrogenase (HLADH).[1] Previous studies from this laboratory indicated substantial tunneling with HLADH at 25 °C using a mutant form of protein that was found to "unmask" tunneling (*9*). The extension of these studies down to −35 °C has been possible through the use of a methanol/water cryosolvent system described earlier by Fink and coworkers (*10*).

As the temperature is reduced below 0 °C, two opposing effects are expected to emerge. First, if protein dynamics

† Supported by a Grant (to J.P.K.) from the National Science Foundation (MCB 9514126).

* To whom correspondence should be addressed.

‡ Present address: Department of Chemistry, Stanford University, Stanford, CA 94305.

[1] Abbreviations: HLADH, horse liver alcohol dehydrogenase; F93W, mutant HLADH that differs from the wild-type enzyme by $Phe^{93} \rightarrow Trp$; TADH, thermophilic alcohol dehydrogenase; KIE, kinetic isotope effect; TLC, thin-layer chromatography; HPLC, high-performance liquid chromatography; MeOH, methanol; MeCN, acetonitrile; DMSO, dimethyl sulfoxide; DMF, dimethylformamide; PrOH, 1-propanol; EGOH, ethylene glycol; MPD, 4-methylpentane-2,2-diol; GlOH, glycerol.

10.1021/bi002075l CCC: $20.00
Published on Web 01/23/2001

can influence the reaction barrier, tunneling may be lost as protein motion is reduced at subzero temperatures. By contrast, as the Boltzmann distribution of molecules with sufficient energy to mount a semiclassical barrier decreases, the only option remaining for the chemical reaction may involve barrier penetration. As we show herein, the latter effect predominates with HLADH down to −35 °C. The relevance of these findings to the interrelationship of protein dynamics and catalysis is discussed in the context of both thermophilic and mesophilic alcohol dehydrogenases.

MATERIALS AND METHODS

Materials. All reagents were used without further purification unless stated otherwise. Reagent- and HPLC-grade solvents ethylene glycol, methanol, 1-propanol, glycerol, dimethyl sulfoxide, dimethyl formamide, and acetonitrile were obtained from Fisher; reagent-grade 2,4-dimethylpentanediol was obtained from Eastman; reagent-grade sodium cacodylate, lithium aluminum hydride, lithium aluminum deuteride (98% D), and semicarbazide were obtained from Aldrich. Reagent-grade benzyl alcohol and benzoic acid were obtained from Fisher. Prior to use, benzyl alcohol was purified by vacuum distillation. Scintillation liquid Ecolite was obtained from ICN. Subzero-temperature bath liquid Thermsil was obtained from Corning. [Ring-^{14}C(U)]benzoic acid (ICN) had a specific activity of 56 mCi/mmol. HLADH was obtained from Boehringer-Mannheim as a suspension in a 20 mM KPi (pH = 7.0) 10% ethanol solution.

Synthesis of [1-$^{1}H_2$]- and [1-$^{2}H_2$]-[Ring-^{14}C(U)]benzyl Alcohol. Lithium aluminum hydride or deuteride (30 mg, 1 mmol) was added to a stirred dry ether solution (5 mL) under nitrogen. The reaction mixture was chilled to 0 °C in an ice bath, and 1 mCi of [ring-^{14}C(U)]benzoic acid (0.018 mmol, 56 mCi/mmol) in 1 mL of toluene was added and stirred for 4 h, until all benzoic acid was converted to benzyl alcohol as judged by TLC. The reaction mixture was quenched by slowly adding 1 mL of ice water (during which hydrogen gas evolved vigorously), followed by the addition of 2 mL of HCl to dissolve the resulting aluminum hydroxide. The aqueous layer was extracted with ether (5 mL × 4), and the combined ether layer was washed with brine and then dried over $MgSO_4$. Concentration in vacuo yielded [ring-^{14}C(U)]-benzyl alcohol (950 μCi, yield 95%). The crude product can be further purified by HPLC, eluting at 14 min on a reverse-phase Rainin C18 column (25 cm long, 100 Å pore, 5 mm o.d.). An isocratic solvent was used (12% CH_3OH, 12% CH_3CN, and 76% water), at a flow rate of 1 mL/min.

Preparation of HLADH. The suspension of commercial wild-type HLADH was centrifuged in a 1.5 mL microcentrifuge tube, and the resulting solid was dissolved in 200 mM KCl, 100 mM KPi buffer (pH = 7.0), followed by a second centrifugation to remove the undissolved solid. The clear solution was passed through a Biorad 10-G desalting column, and the eluent was collected in 1 mL fractions, with the majority of HLADH eluting in tubes 3−5. The wild-type enzyme has an extinction coefficient of 0.455 at 280 nm for 1 mg/mL and a specific activity of 2.7 unit/mg at room temperature. A unit is defined here as the conversion of 1 mM NAD^+/min. The F93W mutant HLADH was expressed and purified according to the procedure described by Park and Plapp (*11*) followed by the desalting column described above. F93W enzyme has an extinction coefficient of 0.603 at 280 nm for 1 mg/mL and a specific activity of 0.33 unit/mg (determined by steady-state kinetics mentioned below).

Methods. (1) Solvent Survey. Solvent systems were created by mixing organic solvents with an aqueous buffer to create a final pH* of 7.0 at 3 °C; the final buffer concentration was 100 mM sodium cacodylate and 200 mM semicarbazide (more semicarbazide has been found to inhibit the enzymatic reaction). The pH* was determined by measuring the pH value of the corresponding cryosolvent solution at 3 °C, using a pH meter. It has been previously shown that the pH* values of most cryosolvent/water mixtures do not fluctuate very much (0.05 between +25 and −50 °C) with temperature (*12*). We find results similar to those of Douzou, in that cryosolvent systems containing 100 mM sodium cacodylate and 200 mM semicarbazide display a constant pH* of 7.0 from 25 down to 0 °C. On the basis of the observations and those in the literature, we assumed that the pH* would remain fairly constant from 0 down to −50 °C.

Freezing points were determined by visual inspection and by the observation of a sharp increase of the UV absorption at 210 nm. Temperatures were recorded using a thermocouple.

Solubility was determined by the apparent clarity of the solution, as well as from UV absorption at 280 nm, upon the gradual addition (10% for each 10 °C reduction in temperature) of an organic solvent to an aqueous buffer solution containing HLADH and NAD^+ (final concentrations of 25 μM and 10 mM, respectively).

The relative rate of the oxidation of cryosolvents by HLADH was determined by studying a 30% solvent system at −20 °C with 25 μM HLADH and 10 mM NAD^+; the reactions were monitored by ΔA_{340} for the formation of NADH, and the observed values were normalized to that of 30% methanol.

(2) Low-Temperature UV/Vis Chamber for Kinetic Analyses. A low-temperature UV/vis chamber was constructed in a Cary 118b spectrophotometer with Cole-Palmer C-Flex tubing and Teflon connectors. Corning Thermsil was used as the bath liquid, which could operate effectively down to −170 °C with a viscosity similar to that of water at room temperature. To prevent condensation in the chamber, it was necessary to introduce cold, dry nitrogen to the interior of the chamber and room temperature, dry nitrogen to the outside of the quartz windows of the spectrophotometer. Nitrogen was cooled in the low-temperature bath by passing the gas through a homemade (15 cm diameter, 100 turns) copper coil. The modified UV/vis chamber can be operated within a very stable temperature range, reaching a minimum of −70 °C.

(3) Steady-State Kinetics and Noncompetitive Kinetic Isotope Effects. Enzyme kinetics were measured at pH* = 7.0 (or pH = 7.0) in 100 mM sodium cacodylate, 200 mM semicarbazide, and 10 mM NAD^+. The temperature was monitored with a thermocouple. Kinetic parameters were determined by following the absorbance increase at 340 nm for the production of NADH ($\epsilon_{340} = 6220\ M^{-1}\ cm^{-1}$). Values of k_{cat} and K_M and their standard errors were obtained by either a nonlinear fit of the expression velocity = k_{cat}[E][S]/(K_M + [S]) or a nonlinear fit of the expression velocity = k_{cat}[E][BzOH][NAD^+]/($K_{i,NAD^+}K_{M,BzOH} + K_{M,BzOH}$[$NAD^+$] + K_{M,NAD^+}[BzOH] + [NAD^+][BzOH]) with the program Kinet-

ics. The error bars on the rate constants for protio- and deuterosubstrates come from the fitting algorithm. The concentration of HLADH active sites of the wild-type and F93W mutant was determined by a comparative Bradford (*13*) and spectrophotometric assay (*14*). Noncompetitive kinetic isotope effects, k_H/k_D, were calculated from ratios of the steady-state parameters for protonated and deuterated benzyl alcohols. The propagation of errors of k_H/k_D were calculated from the standard analytical formula for errors $\Delta(k_H/k_D) = [(\Delta k_H/k_D)^2 + (\Delta k_D k_H/k_D^2)^2]^{1/2}$.

(4) Primary and Secondary Tritium Isotope Effects. The synthesis of tritium-labeled substrates used for competitive isotope-effect measurements was previously reported (*15*). The H/T isotope effects were measured with [ring-^{14}C(U)]-benzyl alcohol (56 mCi/mmol) and [1-^{3}H]benzyl alcohol (16 Ci/mmol), which was randomly tritiated at the benzylic position. The D/T isotope effects were measured with [1,1-$^2H_2$]-[ring-^{14}C(U)]benzyl alcohol (10.9 mCi/mmol or 56 mCi/mmol) and [1-^{2}H,1-^{3}H]benzyl alcohol (35 Ci/mmol), which was also randomly tritiated at the benzylic position. The deuterium content of the [1,1-$^2H_2$]-[ring-^{14}C(U)]benzyl alcohol was determined by mass spectrometry of the urethane derivative to be 98.7 ± 0.3% at C-1 (*10*). The [1-^{2}H,1-^{3}H]-benzyl alcohol was synthesized from [1-^{2}H]benzaldehyde, which was labeled at a level >99.8%, as determined by mass spectrometry (*15*).

The HLADH-catalyzed oxidation of benzyl alcohol with NAD^+ produces benzaldehyde and NADH as products. For isotope-effect measurements, the enzyme-catalyzed production of benzaldehyde was coupled with semicarbazide, which forms benzaldehyde semicarbazone. The coupled formation of the semicarbazone makes the enzyme reaction irreversible at the benzaldehyde product release step. Effective trapping was established by measuring isotope effects at varying enzyme activity, while keeping the concentration of semicarbazide hydrochloride constant. The reaction rate for HLADH was maintained at less than 0.1% of semicarbazone formation. All kinetic isotope effects reported were measured at a pH* or pH of 7.0 in 100 mM sodium cacodylate, 200 mM semicarbazide, and 10 mM NAD^+, unless otherwise stated. The reaction was thermostated to ±0.1 °C in a Neslab ULT-80 cryogenic bath. Typically, a reaction mixture of 2.5 mL was made. The reaction was initiated by the addition of radiolabeled benzyl alcohols. Immediately after mixing, three aliquots (3 × 225 μL) were removed as the t_0 points and quenched with 50 μL of 15 mM $HgCl_2$. During the course of the reaction, a 225 μL sample was also removed for each time point, quenched with 50 μL of 15 mM $HgCl_2$, frozen, and stored desiccated at −80 °C. To obtain a t_∞ point, a final aliquot (225 μL) was incubated with an excess of HLADH (25 μL, 1 mM) for at least 3 days to complete the oxidation reaction; this was then also quenched with 50 μL of 15 mM $HgCl_2$. A typical experiment has three t_0 points, seven time points, and one t_∞ point. After thawing, samples were chromatographed on a reverse-phase Rainin C-18 column with an isocratic buffer (12% CH_3OH, 12% CH_3CN, and 76% water) run at 1 mL/min. Tritiated NADH eluted in the dead volume of the column, benzyl alcohol eluted at around 14 min, and benzaldehyde semicarbazone eluted at around 25 min. Fractions with volumes of 1.5 mL were collected in 20 mL plastic vials, using a fraction collector, and 12 mL of scintillation cocktail was then added to each vial. The vials were counted using an LKB Wallac Rackbeta scintillation counter for 5 min/vial. Isotope effects were calculated using the equations given by Melander and Saunders (*16*):

$$\mathrm{KIE} = \frac{\ln(1-f_t)}{\ln\left(1 - f\dfrac{(^3\mathrm{H}/^{14}\mathrm{C})_t}{0.5(^3\mathrm{H}/^{14}\mathrm{C})_0}\right)} = \frac{\ln(1-f_t)}{\ln\left(1 - f\dfrac{(^3\mathrm{H}/^{14}\mathrm{C})_t}{(^3\mathrm{H}/^{14}\mathrm{C})_\infty}\right)}$$

where f is the fractional conversion of the ^{14}C compound, $f = {}^{14}C_{product}/({}^{14}C_{reactant} + {}^{14}C_{product})$ at time t, $(^3H/^{14}C)_t$ is the ^{3}H to ^{14}C ratio in product at time t, $(^3H/^{14}C)_0$ is the ^{3}H to ^{14}C ratio in substrate at the start of a given experiment, and $(^3H/^{14}C)_\infty$ is the ^{3}H to ^{14}C ratio in product at infinite time (complete reaction).

The factor of 0.5 is due to the random tritiation at the reacting carbon. This was confirmed by the observation that at t_∞ half of the tritium counts were presented in NADT, whereas the other half appeared in benzaldehyde semicarbazone. By a method previously reported (*1*), primary isotope effects were measured by comparing tritium in NADH to ^{14}C in semicarbazide; secondary isotope effects were measured by comparing tritium in semicarbazone to ^{14}C in semicarbazone. Isotope effects can be corrected for protium contamination in the deuterated alcohols using the protium contamination in a phenylurethane derivative of nonradiolabeled deuterated benzyl alcohols, as determined by mass spectrometry (*9*). However, because the contamination is small and somewhat variable, using deuterated benzyl alcohols synthesized in different batches, we have chosen to report uncorrected isotope effects. This may result in slightly elevated k_D/k_T isotope effects, with reduced exponents relating to k_D/k_T and k_H/k_T isotope effects and small underestimates of tunneling. The errors in k_H/k_T and k_D/k_T arose from multiple determinations and are therefore indications of their deviations from averaged values. The exponents are defined as $\ln(k_H/k_T)/\ln(k_D/k_T)$, and the propagations of errors of the exponents were calculated by the standard analytical formula for errors as

$$\Delta(\text{exponent}) = [\{\Delta(k_H/k_T)/[\ln(k_D/k_T)](k_H/k_T)\}^2 + \{\Delta(k_D/k_T)\ln(k_H/k_T)/(k_D/k_T)[\ln(k_D/k_T)]^2\}^2]^{0.5}$$

RESULTS AND DISCUSSION

Solvent Survey. Eight cryosolvents (EGOH, MeOH, MPD, PrOH, GlOH, DMSO, DMF, and MeCN), ranging from 30 to 60% (v/v) in their organic solvent content, were surveyed for their freezing points. It was found that, in general, a 10% change in the composition of the cryosolvent lowered the freezing point 10 °C. Except for MeCN, which freezes at a relatively high temperature, all of the other seven cryosolvents have reasonably low freezing points and can provide a suitable operational temperature. The buffer composition was found to affect the freezing point. For example, the phosphate buffer was found to have a freezing point 5 °C higher than that of the cacodylate buffer, leading to the choice of cacodylate buffer for all studies (*12*).

Enzyme solubility was found to be poor in more hydrophobic solvents, such as propanol, MeCN, and MPD. The solvents MeOH and glycerol gave a fair enzyme solubility, whereas DMSO and DMF solubilized the enzyme well.

Table 1: Steady-State Kinetic Parameters and Isotope Effects for Wild Type HLADH[a]

temp, °C	$k_{cat,H}$, min^{-1}	$k_{cat,D}$, min^{-1}	$^{D}(k_{cat})$	$k_{cat}/K_{M,H}$,[b] mM^{-1}, min^{-1}	$k_{cat}/K_{M,D}$,[b] mM^{-1}, min^{-1}	$^{D}(k_{cat}/K_{M})$
3	2.15(0.05)[c]	1.41(0.08)	1.53(0.09)	1.5(0.1)	0.46(0.06)	3.2(0.5)
−20	0.247(0.003)	0.206(0.007)	1.20(0.04)	0.167(0.006)	0.070(0.006)	2.4(0.2)
−32	0.0626(0.0001)	0.057(0.002)	1.11(0.04)	0.046(0.002)	0.017(0.002)	2.7(0.3)
−42	0.0146(0.0001)	0.0142(0.0002)	1.03(0.02)	0.0103(0.0003)	0.0041(0.0002)	2.5(0.1)
−46	0.0120(0.0002)	0.0114(0.0003)	1.05(0.03)	0.0092(0.0005)	0.0036(0.0003)	2.6(0.3)
−50	0.0095(0.0003)	0.0063(0.0002)	1.52(0.08)	0.0074(0.0007)	0.0017(0.0002)	4.3(0.5)

[a] Conducted in 50% MeOH with 100 mM sodium cacodylate buffer, 10 mM NAD^+, and 200 mM semicarbazide (pH* = 7.0). [b] k_{cat}/K_M for benzyl alcohol. [c] The errors are in parentheses and were calculated as described in the Methods section.

The relative activities of the solvents as substrates for HLADH were also surveyed. In addition to not being a good substrate for HLADH, a suitable solvent system should not be a competitive inhibitor of enzyme activity. Neither DMSO nor DMF could be used, because both solvents were found to strongly inhibit enzyme activity, consistent with previous studies (*10*).

GlOH and PrOH were rejected because of supercooling. Between the two remaining choices, MeOH is superior to EGOH because of its lower activity as a substrate for HLADH. This survey led to the choice of the same cryosolvent as that used by Fink and co-workers in an earlier study (*10*).

Analysis of Wild-Type LADH at Subzero Temperatures. Although wild-type HLADH displays kinetic complexity at room temperature (*9*), precluding an analysis of tunneling, it was thought that a decrease in kinetic complexity with decreasing temperature might permit an observation of tunneling at subzero temperatures. The steady-state kinetics of the wild-type LADH can be observed down to −50 °C. The measured steady-state parameters for both protonated and deuterated benzyl alcohols are summarized in Table 1. The Arrhenius plots of k_{cat} (Figure 1A) and k_{cat}/K_M (Figure 1B) indicate straight lines for both benzyl alcohols. In the earlier study by Fink and co-workers, linear temperature dependencies were also seen (*10*). However, these studies used ethanol as a substrate at subsaturating conditions within a narrow temperature range, making direct comparison with the present studies difficult. The plots in Figure 1 can be compared to previous investigations of linearity of Arrhenius plots for enzyme reactions at reduced temperatures, which have alternately yielded straight lines from 0 to −80 °C (*17*) vs curvature at the protein glass transition temperature of approximately −40 °C (*18, 19*). Interpretation of linearity in Arrhenius plots over extended temperature ranges can be complicated by the contribution of multiple steps to the measured parameter that may vary in compensating ways as a function of decreasing temperature.

The noncompetitive H/D kinetic isotope effects for the wild-type LADH are listed in Table 1 and plotted in Figure 2A,B. It is found that at all temperatures $^{D}(k_{cat})$ is smaller than $^{D}(k_{cat}/K_M)$, indicating more kinetic complexity in $^{D}(k_{cat})$ than $^{D}(k_{cat}/K_M)$. This is likely due to a major contribution from the cofactor release to k_{cat} that is absent from k_{cat}/K_M. The small and declining isotope effects for k_{cat}/K_M indicate a kinetic contribution from alcohol-binding and aldehyde-release steps as well. In fact, $^{D}(k_{cat}/K_M)$ is found to be much smaller than that predicted from room-temperature isotope effects (assuming semiclassical behavior alone). The data also indicate a change at the lowest temperature studied

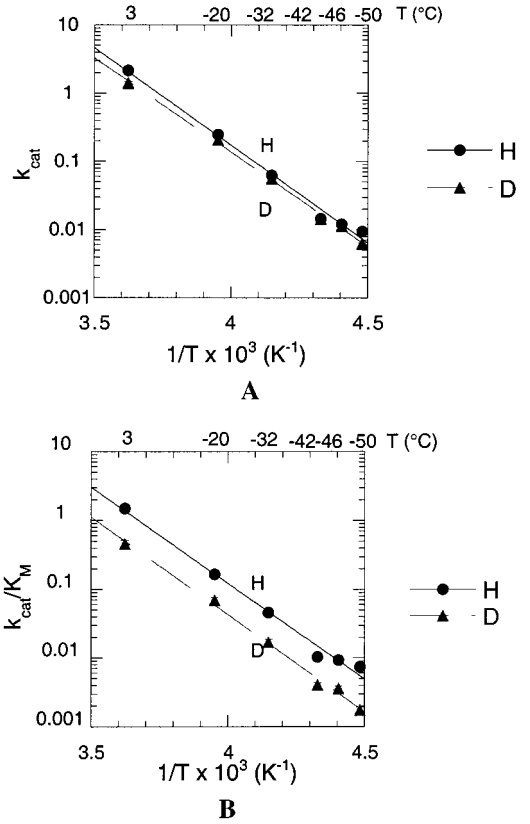

FIGURE 1: (A) Arrhenius plot of k_{cat} for wild-type HLADH-catalyzed benzyl alcohol oxidation at subzero temperatures in 50% MeOH: (●) protonated benzyl alcohol; (▲) deuterated benzyl alcohol. The experiments were conducted in 50% MeOH with 100 mM sodium cacodylate, 10 mM NAD^+, and 200 mM semicarbazide buffer (pH* = 7.0). (B) Arrhenius plot of $k_{cat}/K_{M,BzOH}$ for wild-type HLADH-catalyzed benzyl alcohol oxidation at subzero temperatures in 50% MeOH: (●) protonated benzyl alcohol; (▲) deuterated benzyl alcohol. The experiments were conducted in 50% MeOH with 100 mM sodium cacodylate, 10 mM NAD^+, and 200 mM semicarbazide buffer (pH* = 7.0).

(−50 °C), where isotope effects for both k_{cat} and k_{cat}/K_M begin to increase significantly. This may reflect some interesting behavior (note the proximity to the temperature of the glass transition) but could not be pursued because the MeOH/water solvent mixtures freeze at −55 °C.

Extensive kinetic complexity is further confirmed by the competitive KIEs for the wild-type enzyme (Table 2). As is shown, not only do the KIE values decrease as the temperature is lowered but also the 1° and 2° exponents are considerably below the semiclassical limit of 3.34 (*15*), indicating significant kinetic complexity.

Steady-State Kinetic Parameters and Noncompetitive Kinetic Isotope Effects for F93W HLADH at Subzero

Table 2: Competitive KIE for Wild-Type in 50% MeOH[a]

temp, °C	1° k_H/k_T	2° k_H/k_T	1° k_D/k_T	2° k_D/k_T	1° exp[b]	2° exp[b]
3 (aq)	9.0(0.7)[c]	1.32(0.01)	2.2(0.2)	1.10(0.01)	2.7(0.3)	2.9(0.3)
3 (50% MeOH)	6.7(0.4)	1.23(0.03)	2.2(0.1)	1.08(0.03)	2.4(0.1)	2.6(0.8)
−20	6.1(0.2)	1.20(0.03)	2.3(0.1)	1.13(0.02)	2.2(0.2)	1.4(0.2)
−30	6.6(0.3)	1.30(0.01)	1.8(0.2)	1.14(0.05)	3.2(0.5)	2.1(0.7)
−40	3.0(0.2)	1.12(0.04)	1.5(0.1)	1.09(0.06)	2.9(0.7)	1.3(0.9)
−50	2.2(0.1)	1.25(0.07)	0.99(0.03)	0.99(0.02)		

[a] Conducted in 100 mM sodium cacodylate buffer, 10 mM NAD^+, and 200 mM semicarbazide (pH* = 7.0). [b] Exponent = $\ln(k_H/k_T)/\ln(k_D/k_T)$. [c] The errors are in parentheses and were calculated as described in the Methods section.

Table 3: Steady-State Kinetic Parameters and Isotope Effects for the F93W Mutant of HLADH[a]

temp, °C	$k_{cat,H}$, min^{-1}	$k_{cat,D}$, min^{-1}	$^D(k_{cat})$	$k_{cat}/K_{M,H}$,[b] mM^{-1}, min^{-1}	$k_{cat}/K_{M,D}$,[b] mM^{-1}, min^{-1}	$^D(k_{cat}/K_M)$	$K_{i,H}$,[c] mM	$K_{i,D}$,[c] mM
3	0.80(0.03)[d]	0.72(0.02)	1.12(0.05)	0.54(0.05)	0.15(0.02)	3.5(0.5)	0.33(0.08)	0.8(0.1)
−10	0.282(0.009)	0.234(0.006)	1.21(0.05)	0.21(0.02)	0.055(0.005)	3.8(0.5)	0.27(0.08)	0.9(0.1)
−20	0.108(0.006)	0.090(0.005)	1.20(0.09)	0.061(0.008)	0.012(0.002)	5(1)	0.17(0.07)	0.7(0.2)
−25	0.054(0.004)	0.037(0.002)	1.4(0.1)	0.050(0.009)	0.010(0.002)	5(1)	0.14(0.07)	0.3(0.1)
−30	0.028(0.001)	0.024(0.001)	1.17(0.06)	0.028(0.004)	0.0050(0.0008)	6(1)	0.19(0.09)	1.4(0.4)
−35	0.017(0.001)	0.011(0.001)	1.5(0.1)	0.015(0.002)	0.0020(0.0004)	7.5(2)	0.13(0.04)	1.0(0.3)

[a] Conducted in 40% MeOH with 100 mM sodium cacodylate buffer and 200 mM semicarbazide (pH* = 7.0). The above parameters can be compared with the value in water at 3 °C: $k_{cat} = 3.40 \pm 0.09$ min^{-1}, $^D(k_{cat}) = 2.11 \pm 0.09$; $k_{cat}/K_{M,H} = 16.0 \pm 0.8$ mM^{-1} min^{-1}, and $^D(k_{cat}/K_M) = 5.1 \pm 0.3$. [b] For benzyl alcohol. [c] For NAD^+. [d] The errors are in parentheses and were calculated as described in the Methods section.

Temperatures. Steady-state experiments were conducted with the F93W mutant of HLADH by varying NAD^+ and benzyl alcohol concentrations (both protonated and deuterated benzyl alcohols) in 40% MeOH. Although 50% MeOH had been used for wild-type HLADH, this concentration was found to destabilize F93W. The lowest temperature that could be monitored in 40% MeOH was −35 °C, because of the precipitation of the protein below this temperature.

The F93W mutant has been shown to have little kinetic complexity at room temperature in water (*1*). The steady-state parameters are summarized in Table 3. It was found that the K_M for benzyl alcohol and K_M and K_i for NAD^+ did not change very much as the temperature was lowered. This suggests that the kinetic mechanism does not change as a function of the temperature, down to −35 °C. Although the data fit well to an ordered bi−bi mechanism, a random bi−bi mechanism can also fit the initial rates. As is shown in Table 3, the K_{i,NAD^+} determined with protonated benzyl alcohol is different from that determined with deuterated benzyl alcohol. Because K_{i,NAD^+} is the dissociation constant for the binding of NAD^+ to the enzyme in an ordered kinetic mechanism, this implies a random component to the mechanism. More evidence for a random mechanism is shown below, on the basis of competitive KIEs.

The Arrhenius plots for both k_{cat} and k_{cat}/K_M are straight lines for both protonated and deuterated benzyl alcohols (Figure 3). A curvature in the Arrhenius plot at subzero temperatures would be an indication of tunneling; however, it is possible that the temperature range achievable in these studies is not large enough to observe such a phenomenon. To further understand the behavior of the F93W mutant at subzero temperatures, Arrhenius plots for the isotope effects, $^D(k_{cat})$ and $^D(k_{cat}/K_M)$, were examined (Figure 4). It can be seen that the value for $^D(k_{cat})$ is very small and close to unity. An intrinsic isotope effect for $^D(k_{cat})$ is expected to be much larger than 1, and our observation indicates much kinetic complexity on $^D(k_{cat})$ at subzero temperatures, once again, likely because of slow cofactor release. On the other hand, $^D(k_{cat}/K_M)$ is seen to be significantly larger than 1 but smaller

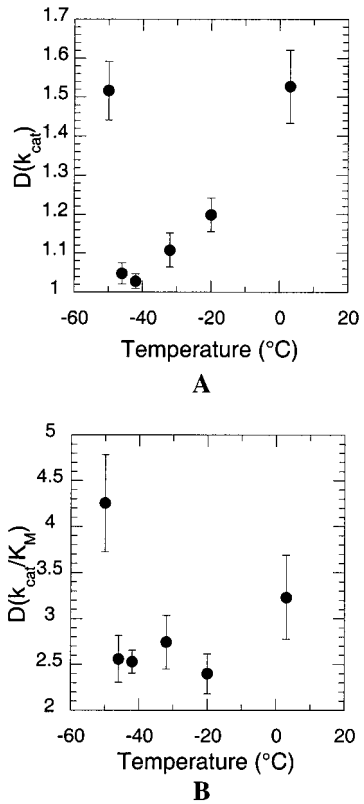

FIGURE 2: (A) Plot of $^D(k_{cat})$ for wild-type HLADH-catalyzed benzyl alcohol oxidation at subzero temperatures in 50% MeOH. $^D(k_{cat})$ decreases as the temperature is lowered until it reaches −50 °C. The experiments were conducted in 50% MeOH with 100 mM sodium cacodylate, 10 mM NAD^+, and 200 mM semicarbazide buffer (pH* = 7.0). (B) Plot of $^D(k_{cat}/K_{M,BzOH})$ for wild-type HLADH-catalyzed benzyl alcohol oxidation at subzero temperatures in 50% MeOH. Like $^D(k_{cat})$, $^D(k_{cat}/K_{M,BzOH})$ also decreases as the temperature is lowered, until it reaches −50 °C. The experiments were conducted in 50% MeOH with 100 mM sodium cacodylate, 10 mM NAD^+, and 200 mM semicarbazide buffer (pH* = 7.0).

than $^D(k_{cat}/K_M)_{calcd}$, according to a semiclassical formulation. The latter calculation was based on the difference between

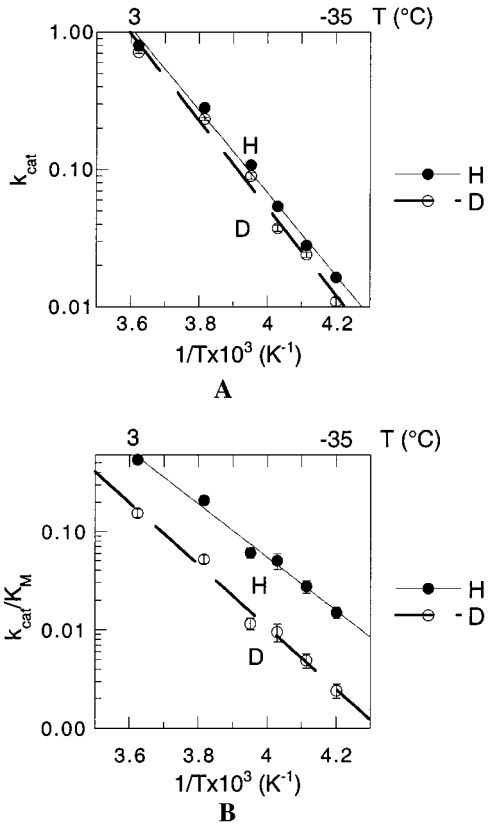

FIGURE 3: (A) Arrhenius plot of k_{cat} for F93W mutant HLADH-catalyzed benzyl alcohol oxidation at subzero temperatures in 40% MeOH: (●) protonated benzyl alcohol; (○) deuterated benzyl alcohol. The experiments were conducted in 40% MeOH with 100 mM sodium cacodylate and 200 mM semicarbazide buffer (pH* = 7.0). (B) Arrhenius plot of $k_{cat}/K_{M,BzOH}$ for F93W mutant HLADH-catalyzed benzyl alcohol oxidation at subzero temperatures in 40% MeOH: (●) protonated benzyl alcohol; (○) deuterated benzyl alcohol. The experiments were conducted in 40% MeOH with 100 mM sodium cacodylate and 200 mM semicarbazide buffer (pH* = 7.0).

the H and D activation energies for F93W at room temperature in water, where it is assumed to have no kinetic complexity (*9*). By contrast, the observed $^D(k_{cat}/K_M)$ for F93W in aqueous solution at 3 °C is very close to the calculated $^D(k_{cat}/K_M)$ value (Table 3). This suggests that the lowered temperature may not change the kinetic mechanism and that it is the presence of 40% MeOH that causes a systematic decrease in the absolute magnitude of isotope effects. This point is pursued further in the context of competitive isotope effects with F93W HLADH (see below).

From the Arrhenius plots, the intercepts (Arrhenius prefactors) and slopes (activation energies) for both protonated and deuterated benzyl alcohols can be obtained. Because there is considerable kinetic complexity associated with k_{cat}, the discussion will be focused on k_{cat}/K_M. The activation energy of k_{cat}/K_M for the protonated substrate with the F93W mutant (11.2 ± 0.7 kcal/mol) is smaller than that for deuterated (12.7 ± 0.9 kcal/mol) benzyl alcohol, and the Arrhenius prefactor isotope effect ($A_H/A_D = 0.015 \pm 0.013$ and $A_H/A_T = 0.33 \pm 0.16$) is far below the semiclassical limit. Although the magnitude of $^D(k_{cat}/K_M)$ may suggest there is more kinetic complexity in methanol/water than water, the unusual Arrhenius prefactor isotope effect implicates tunneling. This observation is discussed in greater detail following the presentation of competitive isotope effects.

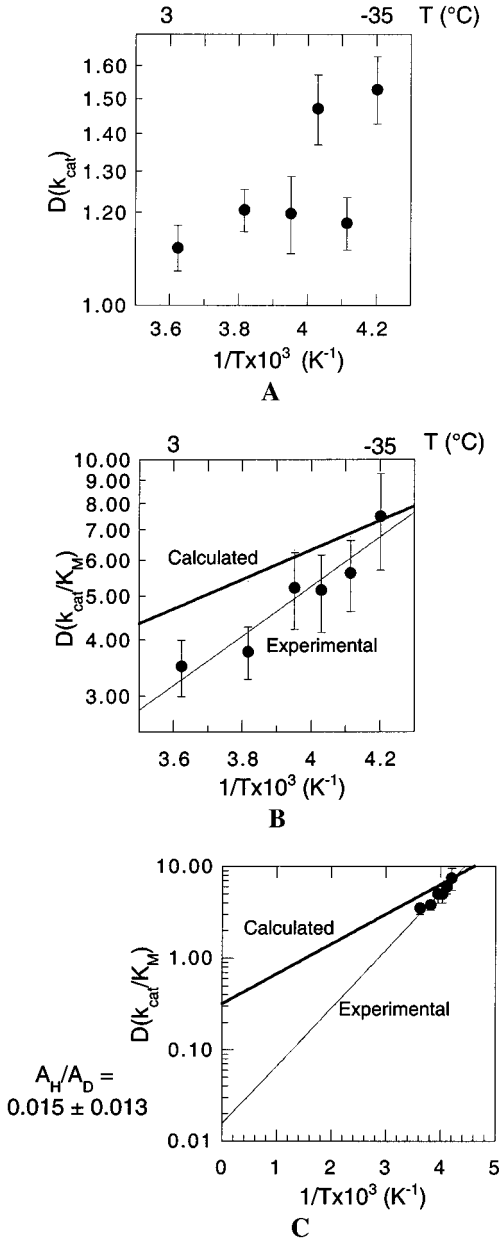

FIGURE 4: (A) Plot of $^D(k_{cat})$ (in log scale) for F93W mutant HLADH-catalyzed benzyl alcohol oxidation at subzero temperatures in 40% MeOH. The experiments were conducted in 40% MeOH with 100 mM sodium cacodylate and 200 mM semicarbazide buffer (pH* = 7.0). (B) Plot of $^D(k_{cat}/K_{M,BzOH})$ (in log scale) for F93W mutant HLADH-catalyzed benzyl alcohol oxidation at subzero temperatures in 40% MeOH. The experiments were conducted in 40% MeOH with 100 mM sodium cacodylate and 200 mM semicarbazide buffer (pH* = 7.0). The solid line, labeled "calculated", is based on the $\Delta H_D^{\ddagger} - \Delta H_H^{\ddagger}$ observed at room temperature. (C) Plot of $^D(k_{cat}/K_{M,BzOH})$ (in log scale) for F93W mutant HLADH-catalyzed benzyl alcohol oxidation at subzero temperatures in 40% MeOH, extrapolated to infinite temperatures. The extrapolated experimental isotope effect on the Arrhenius prefactor, A_H/A_D, is 0.015 ± 0.013.

Competitive Isotope Effects for F93W HLADH at Subzero Temperatures. The averaged competitive KIEs for the F93W mutant at various temperatures in 40% MeOH are listed in Table 4. A typical reaction course is shown in Figure 5. The low percentage of conversion in Figure 5 is due to the extremely slow enzymatic reaction at −30 °C. For higher temperatures, aliquots with a higher percentage of conversion were analyzed, such as 30−70% at 3 °C. The 1° and 2°

Table 4: Competitive KIE for the F93W Mutant of HLADH in 40 and 60% MeOH[a]

temp, °C	1° k_H/k_T	2° k_H/k_T	1° k_D/k_T	2° k_D/k_T	1° exp[b]	2° exp[b]
3 (aq)	10.3(0.2)	1.37(0.01)	2.0(0.1)	1.05(0.01)	3.4(0.3)	6(1)
3 (40% MeOH)	8.6(0.1)[c]	1.35(0.02)	1.80(0.03)	1.07(0.01)	3.65(0.09)	4.4(0.5)
−10	9.4(0.3)	1.32(0.01)	2.05(0.05)	1.04(0.01)	3.1(0.1)	8(2)
−20	10.8(0.1)	1.39(0.02)	2.02(0.07)	1.05(0.02)	3.4(0.2)	7(3)
−30	13.0(0.1)	1.41(0.05)	2.22(0.09)	1.02(0.01)	3.2(0.2)	16(8)
3 (60% MeOH)	8.6(0.4)	1.31(0.02)	1.69(0.06)	1.04(0.04)	4.1(0.3)	7(7)
−20	10.7(0.9)	1.38(0.01)	1.9(0.6)	1.04(0.02)	4(2)	8(4)

[a] Conducted in 100 mM sodium cacodylate buffer, 10 mM NAD, and 200 mM semicarbazide (pH* = 7.0). [b] Exponent = $\ln(k_H/k_T)/\ln(k_D/k_T)$. [c] The errors are in parentheses and were calculated as described in the Methods section.

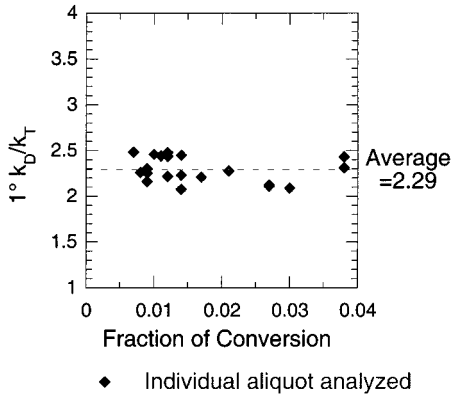

FIGURE 5: Data points for typical competitive KIE experiments with the F93W mutant HLADH: (♦) individual aliquot analyzed. The experiments were conducted in 40% MeOH with 100 mM sodium cacodylate, 10 mM NAD^+, and 200 mM semicarbazide buffer (pH* = 7.0) at −30 °C.

exponents obtained from H/T and D/T KIEs are plotted in Figure 6. It was found that the 1° exponents (Figure 6A) are centered around the semiclassical limit of 3.34, whereas the 2° exponents (Figure 6B) are much higher than 3.34 at all temperatures. The 2° exponent becomes larger as the temperature is lowered, until it reaches a value of 16 at −35 °C. A large 2° exponent of this magnitude is extremely rare, happening only with extensive tunneling. One interesting phenomenon that has been observed previously in the ADH system is that the 2° D/T KIE becomes extremely small (Table 4) with an increased tunneling contribution (*21*). This pattern is repeated at low temperatures: as the temperature is lowered, the decrease in 2° D/T KIEs parallels the increase in the 2° exponents.

The temperature dependence of the primary k_H/k_T is shown in Figure 7, leading to an isotope effect on the Arrhenius prefactor of 0.33 ± 0.16. Analogous to the data obtained from noncompetitive experiments, the value of A_H/A_T is far from the semiclassical value of unity. The above results, when combined with the noncompetitive experiments, support two conclusions: first, that the reaction catalyzed by the F93W mutant does not have significant kinetic complexity at reduced temperatures in the cryosolvent and, second, that the extent of hydrogen tunneling becomes greater as the temperature is lowered from 3 to −35 °C.

Effects of MeOH on the F93W Mutant. Before a consideration of the temperature dependence of tunneling below 0 °C can proceed, it is important to rule out any untoward influence of the cryosolvent on this behavior. One question was whether F93W still follows an ordered bi−bi mechanism in the methanol/water mixture at subzero temperatures, analogous to the enzymatic behavior in water at room

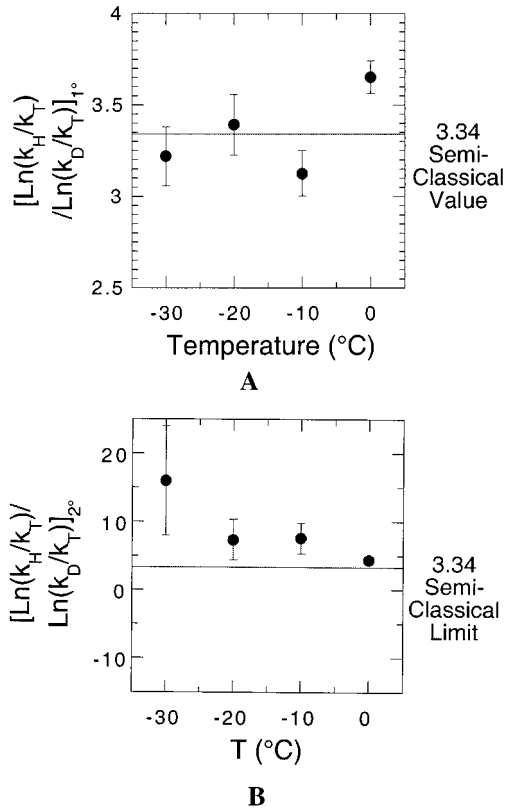

FIGURE 6: Plots of $[\ln(k_H/k_T)/\ln(k_D/k_T)]$, referred to as exponents, for F93W mutant HLADH-catalyzed benzyl alcohol oxidation at subzero temperatures in 40% MeOH. (A) 1° exponents are centered near the semiclassical limit of 3.34. (B) The 2° exponent increases as the temperature is lowered, indicating more tunneling contribution to the reaction rate at lower temperature. The experiments were conducted in 40% MeOH with 100 mM sodium cacodylate, 10 mM NAD^+, and 200 mM semicarbazide buffer (pH* = 7.0).

temperature. The fact that we can fit our steady-state data to an equation for an ordered bi−bi mechanism does not constitute a proof of the mechanism, because random equilibrium mechanisms can also be fitted in this manner (*22*).

A more definitive method to differentiate an ordered bi−bi from a random bi−bi mechanism is by KIE measurements (*18*). In an ordered bi−bi mechanism with cofactor binding first, changes in the NAD^+ concentration should not affect the KIE value because the KIE does not relate to steps before alcohol binding. Table 5 shows the dependence of the KIE on NAD^+ for the F93W mutant; it can be seen that the KIE decreases from 8.6 (at saturating NAD^+) to 6.5 at 0.02 mM NAD^+, which is well below a K_M value of 0.75 mM. This pattern indicates a random component to the reaction, although the fact that the isotope effect does not change

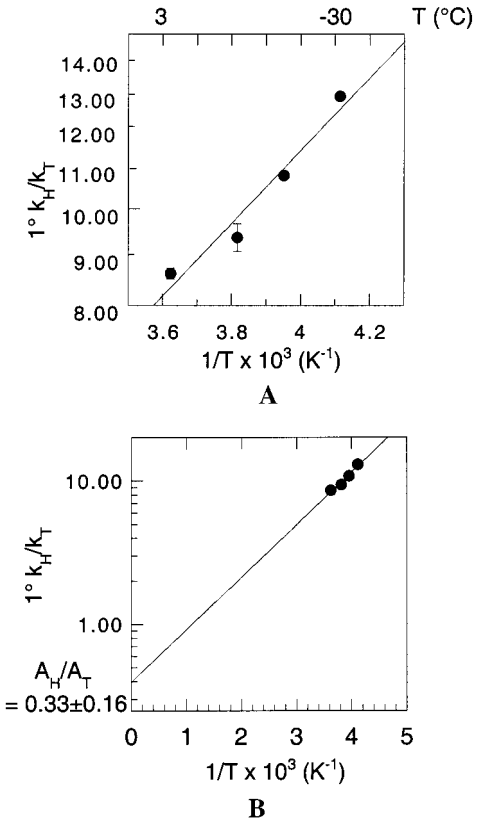

FIGURE 7: Plot of competitive primary k_H/k_T KIEs (in log scale) for F93W mutant HLADH-catalyzed benzyl alcohol oxidation at subzero temperatures in 40% MeOH. (A) 1° H/T plotted in the temperature range of the experiments (3 to −30 °C). (B) 1° H/T extrapolated to infinite temperature. The experiments were conducted in 40% MeOH with 100 mM sodium cacodylate, 10 mM NAD^+, and 200 mM semicarbazide buffer (pH* = 7.0). The extrapolated isotope effect on the Arrhenius prefactor, A_H/A_D, is 0.33 ± 0.16.

Table 5: NAD^+ Dependence of Competitive KIE with the F93W Mutant of HLADH[a]

[NAD^+], mM	1° k_H/k_T[b]	2° k_H/k_T	1° k_D/k_T	2° k_D/k_T
0.02	7.0(0.3)	1.20(0.02)	1.03(0.04)	0.96(0.03)
1.0	7.9(0.7)	1.28(0.03)	1.2(0.1)	1.02(0.01)
10	8.6(0.1)	1.35(0.02)	1.80(0.03)	1.07(0.01)
20	8.6(0.2)	1.32(0.01)	1.80(0.03)	1.02(0.01)

[a] Conducted in 40% MeOH with 100 mM sodium cacodylate buffer and 200 mM semicarbazide (pH* = 7.0), at 3 °C. [b] The errors are in parentheses.

greatly indicates dominance by the pathway in which NAD^+ binds first.

A preferred but noncompulsory ordered bi−bi mechanism is further indicated from the noncompetitive KIE. As is mentioned above, the K_{i,NAD^+} is different for the oxidation of protonated and deuterated benzyl alcohol, indicating some randomness in the kinetic mechanism. If a purely ordered bi−bi mechanism were operative, $^D(k_{cat}/K_{M,NAD^+})$ in the limit of saturating alcohol should be unity. A preferred ordered mechanism with NAD^+ first will result in a finite value for $^D(k_{cat}/K_{M,NAD^+})$ that is smaller than that for $^D(k_{cat}/K_{M,BzOH})$ (*23*).

We note that for the competitive KIE experiments reported in Table 4 the NAD^+ concentration was kept much higher than its K_M, ensuring an ordered bi−bi pathway. In this manner, measurements reflect the interaction of benzyl alcohol with the E−NAD^+ complex.

Another effect of the methanol/water mixed solvent is a reduction in the magnitude of the k_{cat} and k_{cat}/K_M parameters, a feature commonly seen for enzymes in organic solvent mixtures, where k_{cat} and k_{cat}/K_M have been reported to decrease by factors of $10-10^6$ (*12*). Unexpectedly, there is also a decrease in the magnitude of the isotope effects (Tables 3 and 4). We considered the possibility of the increased kinetic complexity in the presence of the mixed solvent as the origin of the reduced isotope effects. As reported earlier, an increase in the kinetic complexity can be detected from a decrease in the 1° exponent to a value below the semiclassical value of 3.34 (*15*, *16*). However, from Table 4, it can be seen that, within experimental error, the 1° exponent at 0 °C in water is similar to that in 40 or 60% MeOH (Table 4), ruling out kinetic complexity as the source of the effect. Although the data are limited for the secondary exponent as a function of MeOH, the magnitude of this parameter appears to be decreasing in concert with the isotope effect itself. One dominant feature of MeOH, along with other cryosolvents, is a role in protein denaturation. It is possible that a partial unfolding of the protein in the organic solvent may be impacting the barrier width of the reaction coordinate, with accompanying changes in both the size of the isotope effects and the extent of tunneling.

Relationship between Temperature and Tunneling for the Mesophilic HLADH. Recently published studies on a thermophilic alcohol dehydrogenase (TADH) with homology to HLADH show a break in the Arrhenius plots at ca. 30 °C for both protonated and deuterated alcohols, with extrapolated isotope effects on the Arrhenius prefactor that go from significantly greater than unity above the break-point temperature to an inverse value upon extrapolation of data below the break-point temperature (*7*). Measurement of the competitive isotope effects, k_H/k_T and k_D/k_T, confirmed the trends in the Arrhenius plots for H and D substrates and led to the conclusion of a decrease in tunneling below 30 °C (*7*). As discussed in some detail by Kohen et al., this behavior is opposite to that expected for chemical systems, in which the contribution of tunneling is predicted to increase with decreasing temperature. An explanation was advanced in which TADH was proposed to "rigidify" at and below 30 °C, such that the dynamic components that are essential for efficient hydrogen tunneling are lost (*7*). This proposal, of a temperature-dependent flexibility of TADH, has been recently confirmed from studies of deuterium exchange into the backbone amides of protein as a function of temperature (*8*).

In this study, we present the first analysis of the temperature dependence of tunneling in a mesophilic enzyme at subzero temperatures. At the beginning of this study, we had anticipated behavior similar to TADH (*7*): specifically, that as the temperature was reduced a point would be reached where the rate of hydride transfer and tunneling would decline in a related manner. Using the F93W mutant of HLADH, where it is possible to study the H-transfer step with little or no contribution from other steps, we have observed a different type of behavior.

First, if we examine the Arrhenius plots for reaction of H and D alcohols (Figure 3), we see linear behavior in the experimental temperature range. Proteins differ in their behavior with regard to subzero temperatures, with some reported to undergo a break in activity at ca. −50 °C, the

"glass" transition (*18*, *19*), whereas others show linear Arrhenius plots down to −80 °C (*17*). These earlier studies have always been complicated by the possible contribution of multiple steps to the measured kinetic parameter or by compensating behavior as a function of temperature. The present studies with HLADH are the first in which it has been possible to look at the temperature dependence of a single step at subzero temperatures. It is clear, nonetheless, that there is no break point down to −35 °C. Unfortunately, because of the properties of the enzyme and cryosolvent used for these studies, it has not been possible to go below −35 °C. It is possible that a break point would be observed at some further reduced temperature.

Despite the limitations of the temperature range available for these studies, our probes of tunneling add another important dimension to the analysis. The cumulative data indicate that once the hydride-transfer step has been isolated, tunneling actually *increases* in a regular fashion as the temperature is reduced from 3 to −35 °C. What do these results imply in the context of our earlier studies with TADH? One possibility is that there is a fundamental difference in the relationship between protein structure and function at reduced temperature for mesophilic and thermophilic proteins. Although an X-ray structure for TADH is not yet available, this seems a highly unlikely possibility, because published comparisons between structures for homologous mesophilic and thermophilic enzymes invariably show very similar three-dimensional structures (*24*).

A far more likely explanation must lie with the response of the reaction coordinate to reduced temperatures. At any given temperature, a hydrogen being transferred has the "option" of proceeding over the top of the classical barrier vs passing through the barrier; the distribution of the behavior will depend on the shape of the barrier and the experimental temperature. The latter controls both the barrier shape itself, which is expected to fluctuate with temperature, and the Boltzmann distribution of molecules with sufficient energy to mount the top of the barrier. As long as the temperature is above a "set point" peculiar to each system, there remains a possibility for over-the-barrier behavior. This is what has been seen with TADH, where reduction of the temperature below 30 °C has been observed to alter protein flexibility and, by inference, barrier shape to such an extent that hydrogen tunneling is reduced. Importantly, at the temperature of the observed break point, there is still sufficient heat partitioned into the protein backbone that hydrogen can pass over the top of the classical barrier. This gives rise to the observed increase in classical transfer at the expense of tunneling at reduced temperatures. The behavior may be expected to become very different at subzero temperatures, where a progressive decrease in protein flexibility is accompanied by a very significant decrease in the fraction of molecules with sufficient energy to mount the classical barrier. In this instance, the only option available for reaction may reduce to one in which the hydrogen *must* pass through the barrier in order to react. This is, in fact, what is commonly observed in chemical systems and appears to be the dominant cause of the behavior of the mesophilic HLADH at subzero temperatures. Thus, even if a break point had been observed in the Arrhenius plots for HLADH below 0 °C, we now consider it highly unlikely that the behavior seen with TADH would be reproduced here. The present results provide beautiful confirmatory evidence for the capacity of HLADH to support a dominant role for tunneling in the hydride transfer between alcohol and cofactor. In addition, these studies suggest that future investigations of the relationship between protein flexibility and hydrogen tunneling may be best approached using proteins from thermophilic sources, allowing correlations to be pursued at elevated temperatures.

REFERENCES

1. Kohen, A., and Klinman, J. P. (1998) *Acc. Chem. Res. 31*, 397.
2. Kuznetsov, A. M., and Ulstrup, J. (1999) *Can. J. Chem. 77*, 1085.
3. Krishtalik, L. I. (2000) *Biochim. Biophys. Acta 1458*, 6.
4. Borgis, D., and Hynes, J. T. (1993) *Chem. Phys. 170*, 315.
5. Antoniou, D., and Schwartz, S. (1997) *Proc. Natl. Acad. Sci. U.S.A. 94*, 12360.
6. Antoniou, D., and Schwartz, S. D. (1998) *J. Chem. Phys. 108*, 3620.
7. Kohen, A., Cannon, R., Bartolucci, S., and Klinman, J. P. (1999) *Nature 399*, 496.
8. Kohen, A., and Klinman, J. P. (2000) *J. Am. Chem. Soc. 122*, 10738.
9. Bahnson, B. J., Park, D.-H., Kim, K., Plapp, B. V., and Klinman, J. P. (1993) *Biochemistry 31*, 5503.
10. Geeves, M. A., Koerber, S. C., Dunn, M. F., and Fink, A. L. (1983) *Biochemistry 258*, 12184.
11. Park, D.-H., and Plapp, B. V. (1991) *J. Biol. Chem. 266*, 13296.
12. Douzou, P. (1977) *Cryobiochemistry*, Academic Press, London.
13. Zubay, G. (1988) *Biochemistry*, Macmillan Publishing, New York.
14. Eklund, H., Plapp, B. V., Samama, J.-P., and Brändén, C.-I. (1982) *J. Biol. Chem. 257*, 14349.
15. Cha, Y., Murray, C. J., and Klinman, J. P. (1989) *Science 243*, 1325.
16. Melander, L., and Saunders, W. H., Jr. (1987) *Reaction Rates of Isotopic Molecules*, Robert I. Krieger Publ. Co., Malabar, Florida.
17. More, N., Daniel, R. M., and Retach, H. H. (1995) *Biochem. J. 305*, 17.
18. Rasmussen, B. F., Stock, A. M., Finge, D., and Petsko, G. A. (1992) *Nature 357*, 423.
19. Brooks, C. L., III, Karplus, M., and Pettitt, B. M. (1988) *Proteins: A Theoretical Perspective of Dynamics, Structure, and Thermodynamics*, Wiley, New York.
20. Saunders, W. H., Jr. (1985) *J. Am. Chem. Soc. 107*, 164.
21. Rucker, J. (1995) Ph.D. Thesis, University of California, Berkeley, CA.
22. Segel, I. H. (1993) *Enzyme Kinetics*, Wiley, New York.
23. Klinman, J. P. (1981) *Crit. Rev. Biochem. 10*, 39.
24. Vieille, C., Burdette, D., and Zeikus, J. (1996) *Biotechnol. Annu. Rev. 2*, 1.

BI002075L